

Major Cellular and Physiological Impacts of Ocean Acidification on a Reef Building Coral

Paulina Kaniewska^{1*}, Paul R. Campbell², David I. Kline¹, Mauricio Rodriguez-Lanetty³, David J. Miller⁴, Sophie Dove^{1,4,5}, Ove Hoegh-Guldberg^{4,5}

1 School of Biological Sciences, The University of Queensland, St Lucia, Queensland, Australia, **2** Agri-Science Queensland, Department of Employment, Economic Development and Innovation, Dutton Park, Queensland, Australia, **3** Department of Biology, University of Louisiana at Lafayette, Lafayette, Louisiana, United States of America, **4** ARC Centre of Excellence for Coral Reef Studies and Coral Genomics Group, School of Pharmacy and Molecular Sciences, James Cook University, Townsville, Queensland, Australia, **5** Global Change Institute, The University of Queensland, St Lucia, Queensland, Australia

Abstract

As atmospheric levels of CO₂ increase, reef-building corals are under greater stress from both increased sea surface temperatures and declining sea water pH. To date, most studies have focused on either coral bleaching due to warming oceans or declining calcification due to decreasing oceanic carbonate ion concentrations. Here, through the use of physiology measurements and cDNA microarrays, we show that changes in pH and ocean chemistry consistent with two scenarios put forward by the Intergovernmental Panel on Climate Change (IPCC) drive major changes in gene expression, respiration, photosynthesis and symbiosis of the coral, *Acropora millepora*, before effects on biomineralisation are apparent at the phenotype level. Under high CO₂ conditions corals at the phenotype level lost over half their *Symbiodinium* populations, and had a decrease in both photosynthesis and respiration. Changes in gene expression were consistent with metabolic suppression, an increase in oxidative stress, apoptosis and symbiont loss. Other expression patterns demonstrate upregulation of membrane transporters, as well as the regulation of genes involved in membrane cytoskeletal interactions and cytoskeletal remodeling. These widespread changes in gene expression emphasize the need to expand future studies of ocean acidification to include a wider spectrum of cellular processes, many of which may occur before impacts on calcification.

Citation: Kaniewska P, Campbell PR, Kline DI, Rodriguez-Lanetty M, Miller DJ, et al. (2012) Major Cellular and Physiological Impacts of Ocean Acidification on a Reef Building Coral. PLoS ONE 7(4): e34659. doi:10.1371/journal.pone.0034659

Editor: Wei-Chun Chin, University of California, Merced, United States of America

Received: September 19, 2011; **Accepted:** March 6, 2012; **Published:** April 11, 2012

Copyright: © 2012 Kaniewska et al. This is an open-access article distributed under the terms of the Creative Commons Attribution License, which permits unrestricted use, distribution, and reproduction in any medium, provided the original author and source are credited.

Funding: This work was supported by the Australian Research Council Centre for Excellence for Coral Reef Studies. The funders had no role in study design, data collection and analysis, decision to publish, or preparation of the manuscript.

Competing Interests: The authors have declared that no competing interests exist.

* E-mail: p.kaniewska@aims.gov.au

These authors contributed equally to this work.

Current address: Australian Institute of Marine Science, Townsville MC, Queensland, Australia

Introduction

Coral reefs are highly productive and biologically diverse ecosystems despite the oligotrophic waters that surround them [1]. They are important to millions of coastal dwelling people across the planet, underpinning industries such as fishing and tourism [2]. Coral reefs appear to be facing a significant increase in local and global stressors [1,3]. Global warming and ocean acidification have recently emerged as key threats to the long-term survival of coral reefs. Rapidly warming oceans are driving an increase in the frequency and intensity of mass bleaching events [3], while steadily acidifying oceans have caused large decreases in the concentration of carbonate ions and potentially the ability of marine calcifiers to precipitate calcium carbonate [4].

High levels of atmospheric CO₂ ([CO₂]_{atm}) and subsequent ocean acidification have been implied as a major factor in several extinction events on coral reefs in geological time [5]. The ocean uptake of [CO₂]_{atm} produces carbonic acid (HCO₃⁻) as the carbon dioxide reacts with water. Protons (H⁺), which are formed due to the resulting dissociation of carbonic acid to bicarbonate ions (CO₃²⁻), react with carbonate ions, forming more HCO₃⁻

and thus reducing carbonate ions available for marine organisms [6]. This decrease in [CO₃²⁻] leads to a reduction in the saturation state of calcium carbonate forms such as aragonite, calcite and high magnesium calcite and thus a reduction in calcification by marine organisms [4,7]. To date, most studies of ocean acidification have focused on its impact on calcification rates [4], as opposed to targeting the physiological processes that lead to the biological deposition of calcium carbonate in these organisms and/or sustain organism health (fitness). It is now clear that overall the predicted reduction in ocean pH and [CO₃²⁻] can be correlated with a decrease in calcification for a diverse range of marine calcifiers, however the response is variable, often non linear and there are inter and intra specific differences [4,8,9]. In addition, for studies conducted in the field, ocean acidification effects can be compounded by ocean warming [10]. Calcification is clearly important, but many other physiological processes may be affected in marine organisms [11,12,13]. By assessing these impacts we can commence unraveling cellular and physiological processes that eventually lead to a decrease in calcification rates. This in turn can provide information to explain currently observed discrepancies in calcification rates, which is important if we are to

understand the full ramifications of rapid ocean acidification for coral reefs. Here, we investigate what physiological processes in *Acropora millepora* are affected by changes in ocean pH, both at the level of the phenotype and gene expression level and show that exposure to high CO₂ drive major changes in gene expression, respiration, photosynthesis and symbiosis for the reef building coral.

Results and Discussion

In a study of 8606 unigenes from the coral *Acropora millepora* exposed to ambient, mid and high CO₂ conditions as predicted by the IPCC (Table 1), we report that increases in dissolved CO₂ after 1 and 28 days affected processes including: metabolism, membrane-cytoskeleton interactions, signaling, translation, transport, calcification, protein folding and apoptosis (Figure 1, Table S1). In total, acidification resulted in 643 differentially expressed transcripts (FDR, 5%); the largest number of these differentially expressed genes are up or down regulated in the high CO₂ treatment compared to the control at day 28. This was also reflected in principal component analysis which showed that high CO₂ corals at day 28 were separated from the other samples implying the greatest variation (Figure S1). Differentially expressed genes were subjected to K-means clustering in order to group genes with similar temporal expression patterns and we identified 6 major synexpression clusters (I–VI) (Figure 1). Transcripts with homology to known genes (352 transcripts, Blastx, E-score cutoff 10⁻⁶) were assigned to gene ontology (GO) categories and subjected to classification analysis to identify enriched GO groups (Figure 2). From the pie charts in Figure 1 which show what major GO categories genes in the synexpression clusters belong to, it is apparent that more changes in cytoskeleton interactions occur in cluster IV, more changes in signaling and catalysis occur in clusters I–III and large changes in transport occur in cluster II. Quantitative real-time PCR of ten representative genes supported the results, where each candidate gene in the qPCR followed the trends found in the microarray data with expression levels either increasing or decreasing in response to high CO₂ conditions (Figure 3, Table S2, S3) compared to control corals at day 28. Changes in response to high and mid CO₂ conditions for day 1, where less gene expression changes occurred, contained many changes in heat shock proteins and signaling which differed from changes at day 28 (Table S1). However, this study only had a single time point at a shorter time scale. It would be useful in future studies to better define changes in gene expression levels within the first few days of exposure, which would require an experiment with several time points within these first few days. It should be noted that this study used small sample sizes (n = 3 for microarray analysis and n = 4 for physiology and qPCR) and that future studies would benefit from greater sample sizes, perhaps a

greater range of differentially expressed genes would be detected, and more robust conclusions drawn from the physiological data.

Changes at the mRNA level, where the majority of differentially expressed genes were found at day 28 in the high CO₂ treatment, were confirmed by physiological measurements (Fig. 4). *Acropora millepora* branches lost *Symbiodinium* cells in response to changes in ocean chemistry, (Figure 4A; Kruskal Wallis test, $H_{2,12} = 7.54, p = 0.023$), where after a 28 day exposure, *Symbiodinium* populations in the high CO₂ treatment were reduced ($1.02 \times 10^6 \pm 5.34 \times 10^4$) to less than half the density compared to control branches ($2.3 \times 10^6 \pm 4.68 \times 10^5$) (Figure 4A). The remaining symbiont cells also became less productive and the photosynthetic capacity (as measured by $P_{\text{net}} \text{ max cell}^{-1}$ and $P_{\text{gross}} \text{ max cell}^{-1}$) was reduced. There was a 60% reduction (Kruskal Wallis test, $H_{2,12} = 8.34, p = 0.015$) in $P_{\text{net}} \text{ max cell}^{-1}$ and a 50% reduction (Kruskal Wallis test, $H_{2,12} = 7.73, p = 0.021$) in $P_{\text{gross}} \text{ max cell}^{-1}$ ($P_{\text{net}} \text{ max} - \text{LEDR}$) in the high CO₂ treatment compared to the control (Figure 4B). Decreasing rates of gross photosynthesis per *Symbiodinium* cell, compounded by reduced *Symbiodinium* populations, may lead to a reduction in photoassimilates translocated to the host coral. These changes are likely to have long-term negative effects on host growth and fecundity, with the prospect of increased susceptibility to disease and mortality, especially if *Symbiodinium* populations fail to recover rapidly [14]. The observed decrease in $P_{\text{gross}} \text{ max}$ is consistent with previous acidification studies [11,15]; however, in our study there was no change in LEDR per remnant *Symbiodinium* cell among CO₂ conditions (Kruskal Wallis test, $H_{2,12} = 1.65, p = 0.437$). This may be due to the application of very different light conditions to Crawley et al [15] which exposed coral to sub-saturation light intensities and only had a short experimental time scale. More importantly, there was a 3-fold downturn in dark respiration per coral surface area (Figure 4C), (Kruskal-Wallis test, $H_{2,12} = 6.71, p = 0.035$), which is typically associated with a decline in host maintenance and/or growth [16]. Rapid growth, either as tissue growth or calcium carbonate deposition necessitates high respiration rates, but the observed reductions in the rate of respiration can suggest suppression of growth rates and/or metabolism. Physiological changes in this study preceded any observable changes in calcification/growth as determined by changes in buoyant weight, as there was no difference in branch calcification/growth rates between the 3 treatments after the 28 day incubation (Kruskal Wallis test, $H_{2,12} = 0.50, p = 0.778$) (Figure 4D), despite the downturn in both energy production and respiration observed in the high CO₂ treatment. This result may reflect that in this case, observable effects on calcification/growth rates require longer experimental incubation, as the buoyant weight technique may be too insensitive to measure the potential small changes in calcification/growth that may have occurred.

Table 1. Carbonate chemistry parameters^a across experimental conditions.

IPCC	pH*	ALK* (μM/kgSW)	DIC* (μM/kgSW)	(Aragonite)	pCO ₂ (matm)	CO ₃ ²⁻ (μmol kg ⁻¹)
Control (present)	8.0–8.2	2281.9±15.8	1832.4±59.4	3.93–5.21	260–440	253.8±17.9
A1B (medium)	7.8–7.9	2260.0±12.6	2165.4±51.0	1.14–3.71	600–790	145.3±33.7
A1FI (high)	7.6–7.7	2283.3±13.5	2345.5±214.4	0.77–2.85	1010–1350	89.5±13.0

*Measured values.

^aParameters were calculated from measured values of pH, total alkalinity (ALK), dissolved inorganic carbon (DIC), temperature (25°C) and salinity (35 ppm), using the program CO2SYS.

doi:10.1371/journal.pone.0034659.t001

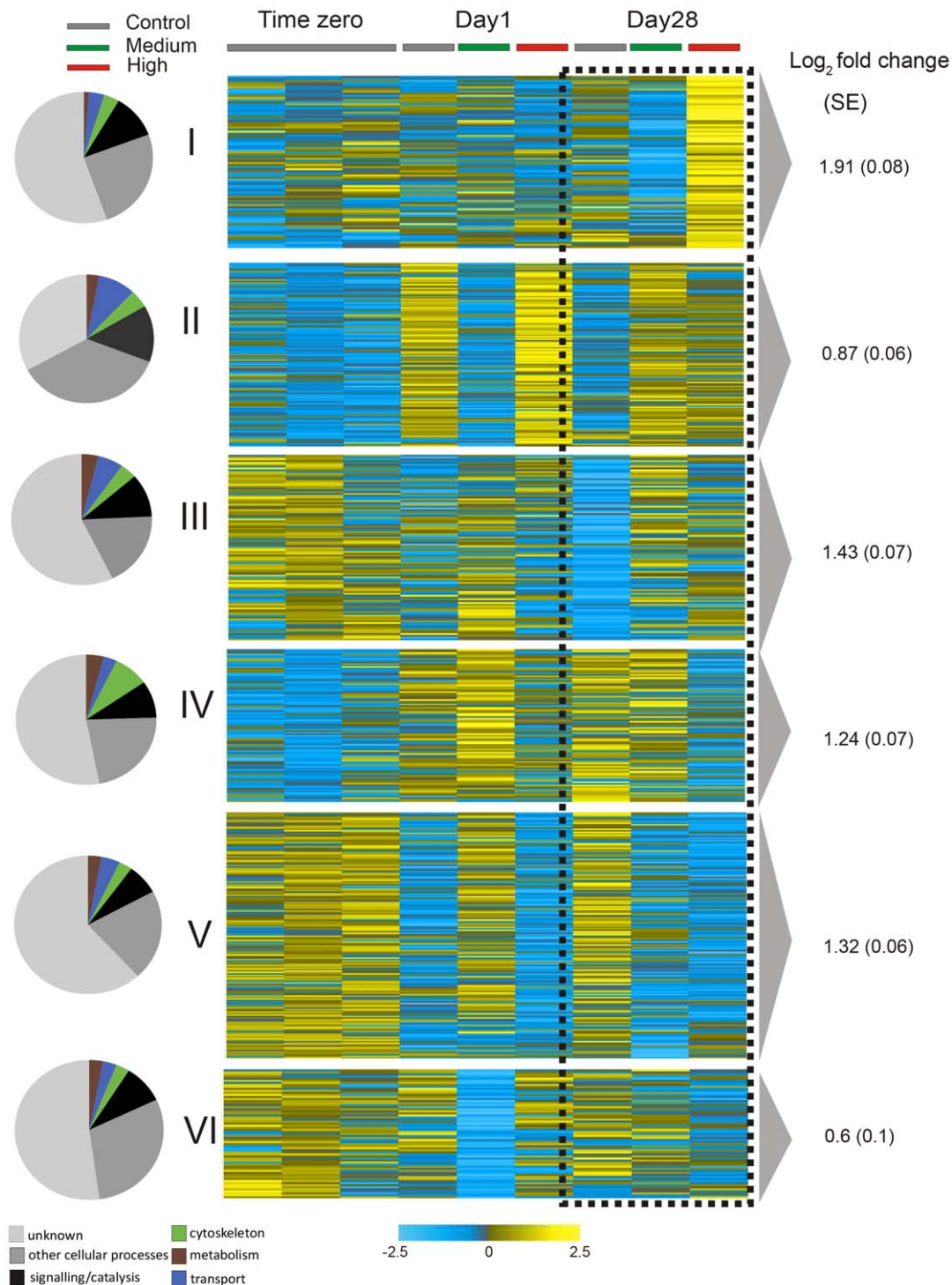


Figure 1. Graphical representation of differentially expressed genes in *Acropora millepora* across pCO₂ treatments (control, medium and high) at day 1 and 28. K-means clustering was applied to group genes (synexpression clusters I–VI) by common temporal expression patterns. Yellow represents upregulation and blue represents downregulation, scale bar is on a log₂ ratio. Each row corresponds to a transcript and each column represents the mean expression (n = 3). For each cluster average log₂ fold changes (±SE) at day 28 are indicated and pie charts classify genes into major biological processes according to enriched GO categories. doi:10.1371/journal.pone.0034659.g001

Metabolism

Changes to metabolic rates are a common outcome of environmental stress [17]. Changes in gene expression suggest that *Acropora millepora* may have reduced its metabolism under high

CO₂ conditions at day 28 (Figure 1 cluster IV–VI, Figure 2, Table S1), mirroring the oxygen flux change (Figure 4). There was an overall down-regulation of genes involved in the tricarboxylic acid (TCA) cycle and the mitochondrial electron transport chain (Table

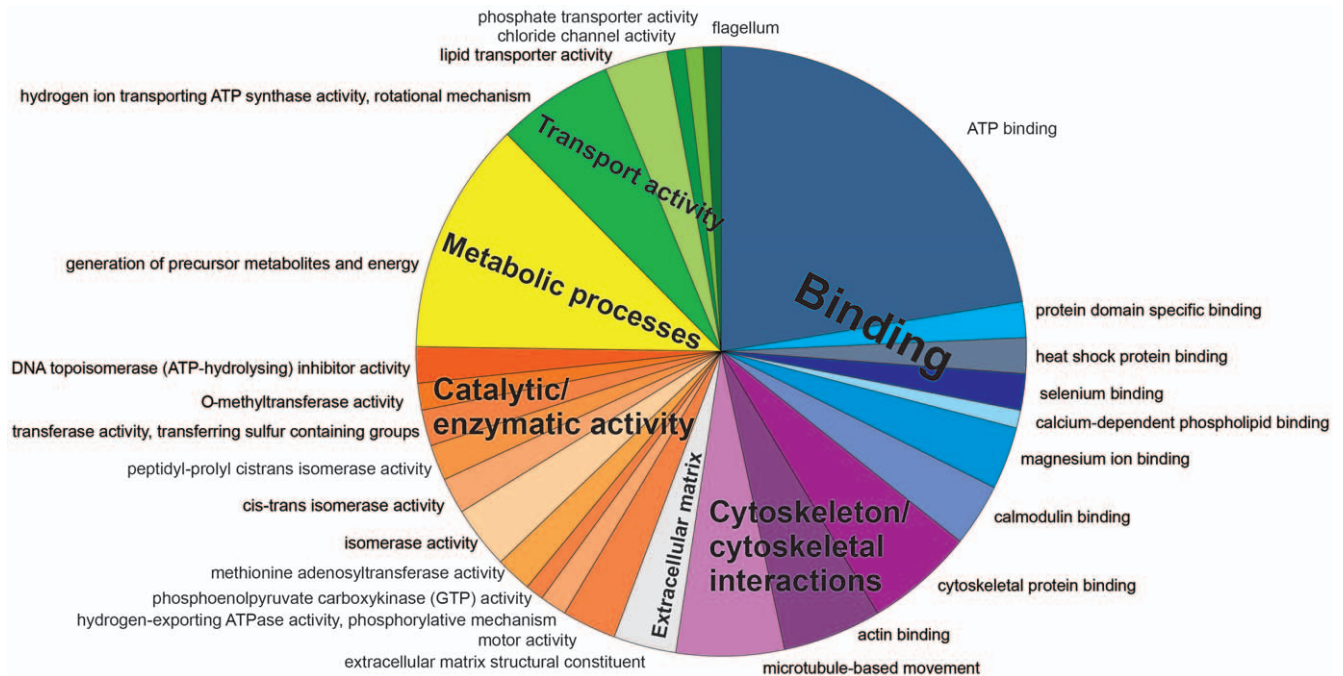


Figure 2. Classification analysis for *Acropora millepora* transcripts that were differentially expressed across pCO₂ treatments (control, medium and high) at day 1 and 28. Gene enrichments ($P < 0.05$) across GO categories are shown. The program GOEAST was used to test for enriched GO categories among differentially expressed genes. Color scheme indicates parent categories (binding, actin cytoskeleton, catalytic activity, metabolic processes and transporter activity) and individual pie segments are annotated for more specific GO categories. The sizes of the pie segments are proportional to the total number of genes enriched. The proportion of differentially expressed genes which were assigned to gene ontology categories was 55%.

doi:10.1371/journal.pone.0034659.g002

S1), indicating reduced oxidative metabolism and capacity to generate ATP and NADPH. There was also an upregulation of triglyceride lipase and Acyl-CoA dehydrogenase (Figure 1 cluster I, II, Table S1), which may point to an increase in the breakdown of lipids for energy use [18,19]. Interestingly, there was an increase in mitochondrial transcripts for ATPase (Figure 1 cluster II, Table S1). Cellular apoptosis is often preceded by an increase in mitochondrial ATPase activity, resulting in an influx of potassium, the activation of caspases and ultimately cell death [20]. Metabolic suppression has been shown in a range of marine organisms in response to CO₂ fluctuations [13,21]. The majority of energy needs in tropical reef building corals are supplied by the photosynthetic endosymbionts [22], but host heterotrophy can occasionally meet host requirements [23]. Depressions in aerobic metabolic activity due to mitochondrial disruptions can undermine the viability of host cells regardless of the trophic source of organic carbon supplied into the TCA cycle. In this particular case, metabolic suppression due to acidosis is likely to have long-term fitness costs.

Acid-Base Regulation and Ion/Macromolecule Transport

Maintaining pH homeostasis is critical to a range of cellular functions [24]. Studies of acid-base regulation and hypercapnia suggest significant physiological challenges for marine fish and worms [13,25]. There are cases where mitochondrial energy production is tied to acid-base regulation through HCO₃⁻ transport [26], bi-direction H⁺ pumping by F₀F₁ ATPase [20], or Na⁺/H⁺ and Cl⁻/HCO₃⁻ transporters on the cell membrane [25]. Membrane proteins play an integral role in: pH homeostasis of the cell, membrane lipid composition and cell shape maintenance [27]. For *A. millepora*, 28 days of high CO₂ conditions resulted in changes in membrane transporters (Figure 1, 2, Table

S1). Specifically, there was downregulation of proton channels (V-type proton ATPases), phosphate transport and protein transport at the cell membrane (Figure 1 cluster IV,V, Table S1). At the same time, sodium and potassium transporters, cell membrane receptors and an ABC transporter were upregulated (Figure 1 cluster I, Table S1). In eukaryotes, ABC type transporters are involved in the export of unwanted molecules, such as toxins [28] from the cell. V-type proton ATPases at the cell membrane serve to acidify the extracellular environment which in turn activates a series of signaling cascades [29]. In the cnidarian ectoderm, plasma membrane proton ATPase activity has been tied to CO₂ uptake [30]. A decrease in this transporter may indicate a decrease in CO₂ uptake under acidification stress. Due to concurrent increases in energy saving ion gradient transporters such as Na⁺/H⁺ exchangers, the decrease in V-type ATPases for proton transport may also be the result of an active suppression of the more costly ATP dependent ion transporters [31]. In addition, a lipid transporter was upregulated in the high CO₂ treated corals at day 28 (Figure 1 cluster II, Table S1), a change not found in acid base regulation of other marine organisms [13,21,25], perhaps implying changes to the lipid configuration of the cell membrane as a response to ocean acidification [32].

Stress Response Mechanisms

Abiotic changes are likely to elicit a cellular stress response (CSR), a universally conserved mechanism to protect macromolecules within cells from the potential damage that physical, chemical or biological stressors may cause. The CSR can increase the tolerance temporarily to the stressor, and remove already damaged cells through apoptosis [33]. Transcripts of *A. millepora* that encode a number of cellular defenses, and transcripts involved

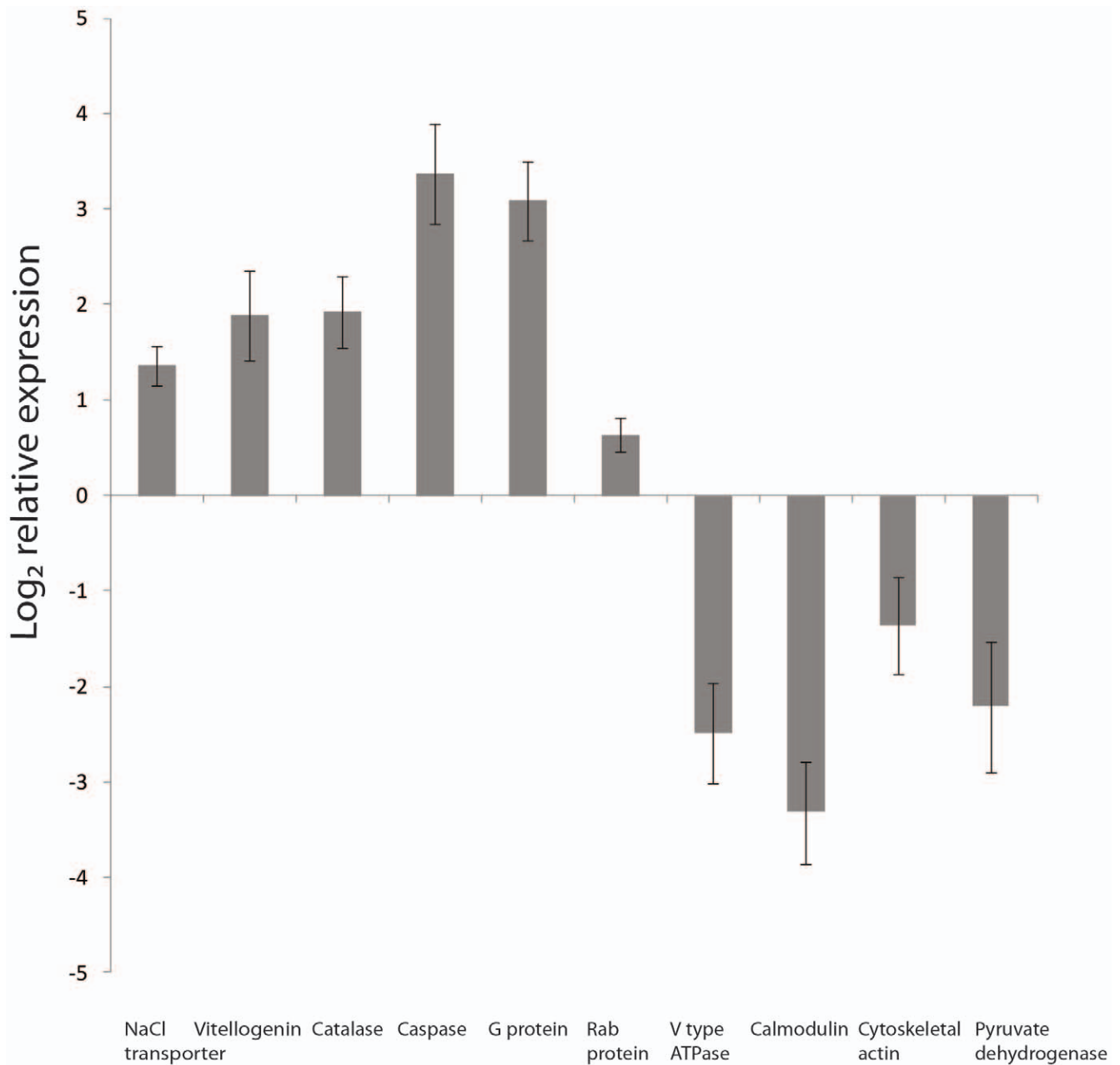


Figure 3. Log₂ relative expression of selected genes using quantitative real-time PCR. Expression levels of genes are plotted as ratio of relative expression of high CO₂ corals versus control corals at day 28. The relative expression for these selected genes was normalized to AdoHcyase and Rbl7. Bars represent standard error of the mean (n=4). doi:10.1371/journal.pone.0034659.g003

in maintenance of protein integrity (molecular chaperones) were downregulated (Figure 1 cluster V, Table S1), whilst genes, protecting the cells against oxidative stress through oxidoreductase activity (eg. Catalase, FAD linked oxidase and selenoprotein [34,35,36]) and involved in apoptosis (caspase 3, TRAF3, p53 inducible protein 11 and programmed cell death protein 4 [37,38,39]), were upregulated in high CO₂ treated corals at day 28 (Figure 1 cluster I, II, III, Table S1). Bcl-2, MALT1 and API-5, potential inhibitors of apoptosis [40,41,42] were downregulated (Figure 1 cluster V, Table S1). The upregulation of apoptotic transcripts is consistent with the upregulation of mitochondrial ATPase described above, which together point to disruption in the mitochondrion leading to cell death [20]. An increase in apoptosis

may reflect that prolonged environmental stress, and either a lack of cell pH homeostasis or elevated maintenance costs, has resulted in cell damage. The loss of *Symbiodinium* cells and an increase in transcripts alleviating oxidative stress may point to impairment in the photosynthetic apparatus in the dinoflagellate symbiont or an impairment of the coral mitochondria [14]. This, in turn, would increase the presence of oxygen radicals in the host tissues and imply cell damage potential. The fact that high CO₂ conditions resulted in overall downregulation of protein folding transcripts, may be a sign that the coral tissue may no longer have the capacity to maintain these integral services. Interestingly, at day one of the high CO₂ treatment there was an upregulation of Heat shock protein 40, a change not found at Day 28 (Figure 1 cluster II,

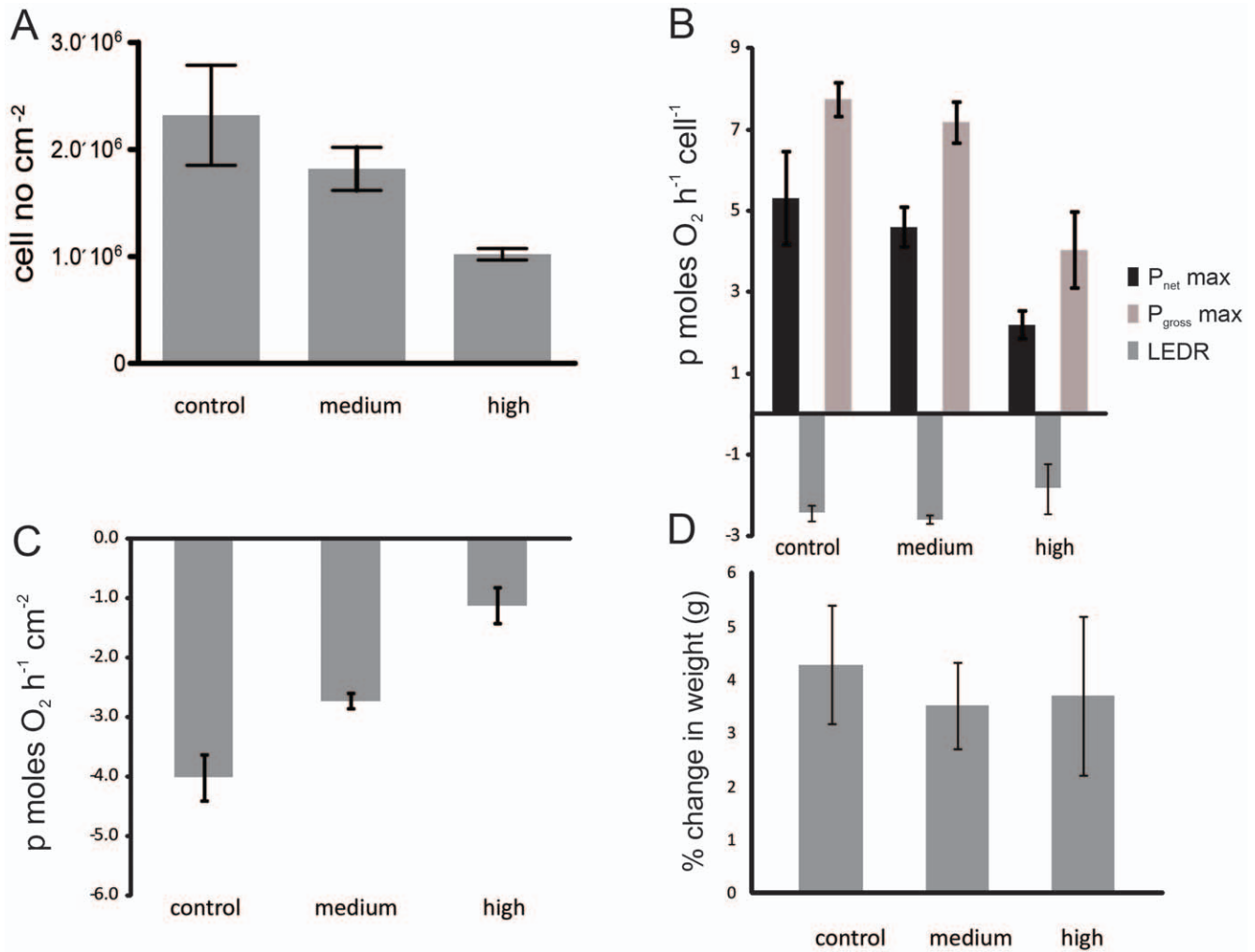


Figure 4. The effect of increasing CO₂ in seawater (control, medium and high) after 28 days on coral-algal physiology. (A) *Symbiodinium* cell number in reef-building coral, *Acropora millepora* (B) photosynthetic capacity per symbiont cell measured as P_{net} max, light enhanced dark respiration (LEDR), and P_{gross} max (P_{net} max - LEDR) (C) dark respiration (R_{dark}) and (D) relative calcification/growth as % change in weight (g) of coral branches over the 28 day experimental period. Error bars represent the standard error of the mean (n=4). doi:10.1371/journal.pone.0034659.g004

Table S1). It must be noted however, that the two other main heat shock proteins (hsp) were not differentially expressed between treatments (hsp 70 and 90) but were maintained at a high expression levels, and their presence may be sufficient for the integrity of newly made proteins. Calnexin and alpha mannosidase transcripts were upregulated (Figure 1 cluster II, Table S1) which would increase the quality control and protein folding ability in the endoplasmic reticulum for proteins that will then be further transported to the golgi complex [43,44]. It is possible that the other downregulated chaperones could be temporarily reduced while awaiting more favorable environmental conditions. A coral c-type lectin, which is involved in innate immunity in corals [45] was downregulated (Figure 1 cluster V, Table S1) under high CO₂ conditions, indicating that this cell stress response may not be responding appropriately, and this decrease may compromise the coral further as in a stressed holobiont, susceptibility to pathogens may increase [46].

Ca²⁺ Ion Binding/Transport and Cell Communication

Several calcium (Ca²⁺) ion binding proteins were downregulated in high CO₂ treatments at day 28 (Figure 1 cluster IV, V, Table

S1). Transcripts for calcium-binding receptors that are potentially involved in innate immunity [47,48] were also suppressed, implying an adverse change in signaling potential at the cell membranes. Downregulation of calmodulin, FKBP12 and EGF-hand proteins also implies potential disruption in cell calcium homeostasis [49,50,51], as these calcium binding proteins control the Ca²⁺ release from ryanodine receptors (RyR) within the endoplasmic reticulum (ER), which is an intracellular Ca²⁺ storing organelle [49,50,51,52]. Calpain, an important Ca²⁺ activated protease that has roles in membrane-cytoskeleton interactions, signal transduction, cell differentiation and apoptosis [53], was upregulated. Changes in these calcium binding proteins indicate that certain signaling pathways may have been altered.

Membrane-Cytoskeleton Interactions

Exposure to high seawater CO₂ concentrations for 28 days resulted in several differentially expressed genes involved in membrane-cytoskeleton interactions and cytoskeletal remodeling (Figure 1, 2, Table S1). It is possible that the change in regulation of these transcripts reflects a change in proteins involved in cytoskeletal interactions, cytoskeletal organization, intracellular

transport, cell shape integrity and cell motility [54,55] [55]. Specifically, there was downregulation of cytoskeletal actin 1, centractin, radixin and coatomer epsilon subunit and radixin (Figure 1 cluster IV, V, Table S1), whilst there was upregulation of tubulin and Lgl tumor suppressor unit (Figure 1 cluster I, II, Table S1). The actin cytoskeleton is important in a diverse range of processes such as cell motility, contractibility, mitosis and cytokinesis, intracellular transport, endocytosis and secretion. In addition, it has been suggested that actin is also involved in regulation of gene transcription through changes in the cytoskeletal actin dynamics or assembly of transcriptional regulatory complexes [55]. Actin is also an important part of the nuclear complex being required for the transcription of RNA polymerases and is also involved in the export of RNAs and proteins from the nucleus [55]. It is possible that the downregulation of cytoskeletal actin in high CO₂ conditions reflects a change in the regulation of gene transcription of proteins involved in cytoskeletal interactions. In addition this downregulation can imply changes in the intracellular transport, plasma membrane interactions and cell shape/integrity. There was also an upregulation of alpha tubulin, which forms a constituent of the microtubule filaments, involved in cytoskeletal organization and vesicle transport. Downregulation of coatomer epsilon subunit implies changes in protein trafficking between the endoplasmic reticulum and the Golgi complex, while upregulation of Lgl tumor suppressor unit indicates changes to events controlling cell polarity [56,57]. Cell volume control changes have been recorded in other marine organisms such as crabs in response to hypercapnia [58], and similar changes may be occurring in the stressed coral cells. The downregulation of Radixin, an important protein involved in linking the plasma membrane to the cytoskeleton using actin rich surfaces [59], supports the downregulation of cytoskeletal actin. Centractin, or Actin Related Protein 1 (ARP1), was also downregulated under higher CO₂ stress, and this is an important activator of cytoplasmic vesicle movement [60]. In contrast, at day one in high CO₂ stressed corals, there was an upregulation of Radixin and Centractin, or Actin Related Protein 1 (ARP1) (Figure 1 cluster VI, Table S1), indicating that different changes in cytoskeletal interactions were occurring at this stage. The cytoskeleton has profound effects on the plasma membrane. At times, there may be uninhibited lateral diffusion of lipids and proteins across the plasma membrane; the influx of these molecules can be regulated by the membrane-cytoskeleton links. These become obstacles to free diffusion through diffusion-limited lipid domains [54]. It may be that changes in these membrane-cytoskeleton links in this study reflect changes in transport across the membrane.

Rab/Ras GTPases

Exposure to increased CO₂ concentrations for 28 days lead to an up (Figure 1 cluster II, Table S1) and downregulation (Figure 1 cluster V, Table S1) of transcripts that resemble members of the Rab/Ras GTPases families (small G-proteins). The Ras GTPase superfamily is a small monomeric group of GTPases, which are involved in cell proliferation and cell signaling events in response to external stimuli. Disruption of the Ras signaling pathway is a key component in the progression of tumor growth [61]. The Rab GTPase family is part of the Ras GTPase superfamily and plays a key role in many membrane-trafficking events in eukaryotic cells, such as exocytosis. This group of proteins which tightly associates with the cell membrane is involved in transport vesicle formation, actin and tubulin motility, docking and membrane fusion. Rab proteins are active when bound to GTP and are inactive when bound to GDP [62,63]. In its active state, the Rab protein

regulates the transport of lipids and proteins between distinct membrane bound organelles through interactions with downstream effector proteins which are recruited onto the membranes [63]. Small G-proteins are implicated in most cellular events where plasma membrane-cytoskeleton interactions or plasma membrane shape changes (plasma membrane deformations) occur. The observed upregulation in members of these small monomeric GTPases most likely reflects changes in the cell membrane and cytoskeletal interactions to accommodate changes in external seawater chemistry.

Extracellular matrix

Changes in the extracellular matrix (ECM) have previously been implied to potentially affect calcification [34,36]. Our expression patterns indicate that only two transcripts encoding previously described ECM proteins changed after 28 days under mid CO₂ exposure. SEC13L1 was upregulated (Figure 1 cluster III, Table S1) while peroxidase was downregulated (Figure 1 cluster IV, Table S1). At day 28 under high CO₂ exposure, there was also a downregulation to a predicted protein in the extracellular matrix (Table S1). This implies that small changes to calcification may have started occurring and that perhaps with a longer experimental incubation time more ECM and calcification related transcripts would have been differentially expressed. This overall supports our findings at the phenotype level where no change in calcification/growth was found (Figure 4). Overall in this study there were fewer changes in transcripts which may be involved in calcification, in response to ocean acidification, compared to gene expression studies with corals exposed to thermal stress where changes to the following transcripts were observed; collagen α -1, ECM matrix metalloprotease, papilin, carboxypeptidase inhibitor SmC1, procollagen, galaxin and SCP-like extracellular protein [34,36].

Cell-wide Responses by Corals to Ocean Acidification: A Model

To highlight the differences between acidosis which may be a factor in this study from the impact of hypercapnia seen in other marine organisms, we propose a model (Figure 5) of cell-wide, coral host response to high CO₂ stress. This model attempts to account for the classic acidosis response (acid-base regulation and metabolic depression) and the novel responses observed in the studied coral (apoptosis, signaling events, calcium homeostasis, cytoskeletal remodeling, cytoskeletal-membrane interactions and oxidative stress). The coral specific responses may result from increased reactive oxygen species (ROS) and/or increased reactive nitrogen species (RNS) created from a disturbance in the *Symbiodinium* cell, the host mitochondria, or both [14,34]. Upregulation of catalase, FAD-linked oxidase and selenoprotein indicates that there may be an increased amount of ROS in the coral cells [64,65]. Increased ROS/RNS can result in a disruption to the calcium homeostasis [34]. The role of internal [Ca²⁺] increase in coral bleaching has been suggested previously [34]. The downregulation of calmodulin (CaM), FKBP12 and EF-hand proteins under high CO₂ stress indicates that there may be a disruption to the Ca²⁺ homeostasis [49,50,51]. Modifications of the actin cytoskeleton, membrane-cytoskeleton interactions and cell receptor/adhesion properties will be affected by a disruption in Ca²⁺ homeostasis and metabolic suppression [34,66]. Both oxidative stress and an increase in intracellular Ca²⁺ can lead to apoptosis and changes in transcripts indicate that both the NF- κ B and p53 apoptotic pathways [67,68] were upregulated. Changes in predicted proteins in the extracellular matrix may imply changes in or restructuring of the extracellular matrix. Our model suggests

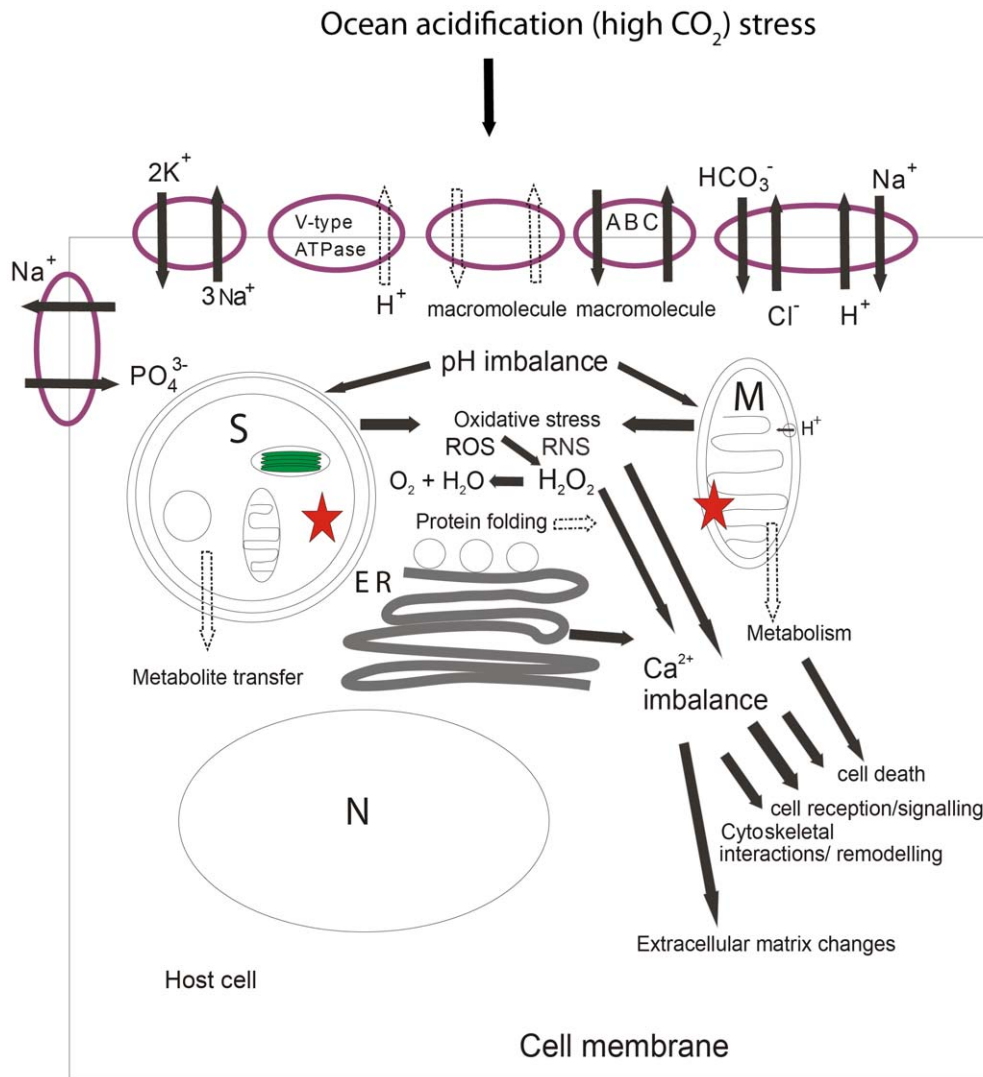


Figure 5. A proposed model of cellular events occurring as a result of ocean acidification. These changes lead to compromised health in *Acropora millepora* (reduction in symbiont cells and decreased photosynthesis and respiration). The schematic depicts an endodermal cell which contains the symbiont cell. Cellular events depicted here are likely to also occur in other cell types which do not contain symbionts, especially the acid base changes at the cell membrane. Changes in carbonate chemistry lead to changes in acid base regulation and cell membrane transporters. Acid base regulation may not be sufficient leading to acidosis within the cell. This could increase reactive oxygen species (ROS) due to a disruption (☆) in the *Symbiodinium* cell (S) and/or in the coral host mitochondrion (M), which may also produce reactive nitrogen species (RNS). The overall oxidative stress and a disruption to calcium stores at the endoplasmic reticulum (ER) can lead to calcium imbalance. This in turn leads to events such as changes in the extracellular matrix, cytoskeletal remodeling, changes in cytoskeletal interactions, disruption to cell reception and signaling potential, and an increase in cell death. Moreover disruption in both the host mitochondrion and *Symbiodinium* cell leads to a decrease in metabolism and a decrease in metabolite transfer from the symbiont cell. In addition the disruption in the host mitochondrion can also lead to cell death. For the cell membrane transporters black arrows indicate upregulation and white arrows indicate downregulation.
doi:10.1371/journal.pone.0034659.g005

that similar cellular events are occurring under acidosis induced bleaching to those reported for thermally induced bleaching [14,34,36], but with the addition of changes to acid-base regulation and mitochondrial ATPase activity.

On our present greenhouse trajectory, we are likely to use all the >4000 Gt of carbon present in the global fossil fuel reserves by 2400. This will significantly acidify the oceans for thousands of years [69] and take them to a point not seen in tens of millions of years [70]. Our study highlights the imperative to investigate the impacts of ocean acidification on processes other than those involved in biomineralisation. Also, there is a need for more studies investigating the effects of naturally occurring changes in pCO₂ on marine calcifiers *in situ*. This is a priority, if we are to

understand the fate of the many supporting roles that corals contribute to the maintenance of coral reefs.

Materials and Methods

Experimental Design

A total of 20 branches (7–8 cm long) were collected from 4 healthy colonies of the reef building coral *Acropora millepora* on Heron Island Reef flat (23°33'S, 151°54'E), Great Barrier Reef, Australia. Coral branches were affixed onto cut 15 mL falcon tubes using Selleys Knead It Aqua (Padstow, Australia) and Selleys autofix super glue (Padstow, Australia). The affixed branches were then placed onto a rack which was deployed back to the Heron

Island reef flat, where they remained for 4 weeks, exposed to natural light and flow regimes in order to recover from handling. Following this acclimation period they were transferred to aquaria with running seawater and under ambient light (with shade cloth see below) and ambient temperature (26°C) conditions for 10 days. For each treatment there were four randomly distributed aquaria and for each *A. millepora* colony, branches were evenly distributed across treatments, with 6 branches per colony in each of the treatment tanks (ambient, mid and high – see below). Branches were designated to be used either for respirometry assays and physiology measurements or microarray analysis. The experiment was run for 28 days and coral branches were sampled, snap frozen in liquid nitrogen and stored at -80°C for later analysis at time zero, day 1 and day 28. For each time point, two branches per colony were sampled and one branch was used for physiology and one branch was used for genomic analysis.

The experimental set up consisted of 12 (4 aquaria per treatment) flow-through aquaria (80 L) under natural light and a layer of shade cloth which resulted in photosynthetically active radiation levels of a maximum of $859.6 \mu\text{mole quanta m}^{-2} \text{s}^{-1}$ and a daily average level of $433.6 \pm 8.6 \mu\text{mole quanta m}^{-2} \text{s}^{-1}$ for the light period of the day. Aquaria were supplied with unfiltered seawater which was being pumped straight from the reef flat on Heron Island into CO_2 mixing tanks, and then distributed across aquaria. The control aquaria were receiving seawater from the Heron Island reef flat where the natural diurnal variability in pH ranged between 8.0–8.2 due to tidal changes and metabolic activity on the reef flat, which corresponded to a pCO_2 range of 260–440 ppm. The pCO_2 ranges in the two acidification treatments were controlled by a CO_2 dosing control system (Aquacontroller III, Neptune Systems, Carlsbad, CA, USA) which used pH readings in the large 300 L CO_2 mixing tanks, to either open or close solenoid valves (Dupla Australia, Littlehampton, Australia) and would control the amount of CO_2 being added to the mixing tanks. The medium CO_2 treatment was controlled to a pH target of 7.8–7.9 corresponding to 600–790 ppm. The high CO_2 treatment was targeted to a pH range of 7.6–7.7 corresponding to 1010–1350 ppm. Temperature, pH and light levels were recorded throughout the experiment and total alkalinity across control and CO_2 treated aquaria was determined with a Mettler Toledo T50 automated titrator, with 0.1 M HCl and 130 g seawater samples using the Gran titration method in a two-stage, potentiometric, open-cell titration following the method of [71]. Acid concentrations and the alkalinity measurements were calibrated at the beginning of each run using Dickson certified reference sea water standards (Andrew Dickson, SIO, Oceanic Carbon Dioxide Quality Control). Dissolved Inorganic Carbon (DIC) was sampled into 50 mL glass vials after filtering with a $0.45 \mu\text{m}$ syringe filter, fixed with $15 \mu\text{L}$ saturated mercuric chloride and then sealed with a rubber lid and aluminum cap (Wheaton, USA). DIC samples were then run on a custom DIC system with a LICOR gas analyzer (Rob Dunbar lab, Stanford, USA) with a Dickson sea water reference run every 7 samples. Carbon species concentration and aragonite state were determined for each treatment using the CO2SYS program using the dissociation constants from [72] and refit by [73] using TA, DIC, pH, and temperature measurements [74].

Respirometry Measurements

Coral branches designated for physiological measurements were used for respirometry assays. The coral branches were dark adapted for at least an hour before respirometry assays, which were performed after dusk. Branches were placed in 70 cm^3 clear acrylic chambers with an inserted optode sensor connected to an

Oxy4 v2 system (PreSens, Regensburg, Germany). The chambers were placed within an acrylic container (on top of a magnetic stirrer), which was connected to a water bath keeping the temperature constant throughout the assays at 26°C , the ambient water temperature at Heron Island during the course of the experiment. Chambers were filled with seawater from respective experimental treatments in the aquaria. Photosynthesis vs irradiance curves (P-E curves) were conducted by using the actinic light source of an imaging pulse amplitude modulation fluorometer (iPAM, Walz, Effeltrich, Germany), and exposing coral branches in chambers to 0, 10, 20, 55, 110, 925 $\mu\text{mole quanta m}^{-2} \text{s}^{-1}$ for 10 min and then followed by exposure at 1075 and 1250 $\mu\text{mole quanta m}^{-2} \text{s}^{-1}$ for 5 min each, and the run was concluded by a 10 min incubation at 0 $\mu\text{mole quanta m}^{-2} \text{s}^{-1}$. Respirometry rates were normalized to cell number and coral surface area. The exposure to different light levels enabled the calculation of P-E curve parameters [75] following methods in [15]; dark respiration (R_{dark}) estimated from the initial 10 min dark incubation, sub-saturation photosynthetic efficiency (α) derived from the regression line slope of the low irradiance levels (10, 20, 55, 110 $\mu\text{mole quanta m}^{-2} \text{s}^{-1}$) in relation to the estimated E_k , photosynthetic capacity ($P_{\text{net max}}$) was estimated as the greatest rate of oxygen evolution at the high irradiance levels (925, 1075, 1250 $\mu\text{mole quanta m}^{-2} \text{s}^{-1}$), and finally light-enhanced dark respiration (LEDR) was determined from the oxygen consumption in the last dark incubation post irradiance exposure.

Population Density and Chlorophyll *a* Content of *Symbiodinium*

The cell density and pigment content of *Symbiodinium* were measured by removing tissue from coral fragments by air-brushing frozen fragments in 5 mL 0.06 M phosphate buffer (pH 6.65). The homogenate was centrifuged at $4000 \times g$ for 5 min. The supernatant was removed and the remaining dinoflagellate pellet was re-suspended in filtered seawater ($0.45 \mu\text{m}$) and separated into aliquots that were used for pigment quantification and *Symbiodinium* cell counts. *Symbiodinium* pigment quantification aliquots were centrifuged at $4000 \times g$ for 5 min, the supernatant was removed and 1 mL of 100% cold methanol was added to the pellet. The solution was sonicated on ice cold water for 10 min and then centrifuged at $4000 \times g$ for 5 min. The supernatant was collected and transferred into a tube. This process was repeated until complete pigment extraction was achieved (when the final supernatant was clear). The total final extracted solution was filtered ($0.45 \mu\text{m}$) and used for pigment separation in a Shimadzu SCL – 10 HPLC linked to a Shimadzu SPD – M10A photodiode array detector, using the column and method described in [76] with solutions A (methanol: acetonitrile: aqueous pyridine, 50:25:25 v:v:v) and B1 (methanol: acetonitrile: acetone, 20:60:20 v:v:v). A standard for methanol extracted pigment chlorophyll *a* was used for quantifying pigments and normalized on a per cell basis. *Symbiodinium* cell counts were estimated using eight randomly selected replicates counted using a haemocytometer (Boeco, Germany) on a Zeiss standard microscope; the counts were normalized to coral surface area in cm^2 , as obtained by dipping coral fragments into paraffin wax following the method of [77].

Coral Growth Rate Estimation

Acropora millepora branch growth/calcification rate was estimated using the buoyant weight method [78]. Coral branch weights for samples across treatments were measured at time zero, day 1 and day 28. The branches were suspended by a thin fishing line below a precision balance (Mettler Toledo) and the weight was recorded. The growth/calcification rate was calculated as a relative unit by

subtracting the initial weight (g) from the final weight (g) and converting this to a percent change in weight over the course of the experimental period.

Statistical Analysis

All data were tested for normality and homogeneity of variance and where assumptions were violated, the data were corrected by transformations. Non-parametric equivalents of tests were used in cases where assumptions were violated despite transformations. A Kruskal Wallis test was used to determine the effect of changes in CO₂ concentrations on *Symbiodinium* density, branch calcification/growth, P_{net} max, P_{gross} max, LEDR and R_{dark}. To test for significance on the expression levels of mRNAs from quantitative real time PCR between control and high CO₂ levels, for each gene a Welch t-test was used. All statistical analyses were performed using STATISTICA 7.0 (Statsoft Inc., Tulsa, USA).

Microarray Description

The microarrays used in this experiment were printed at the Adelaide Microarray Facility (Australia) and consisted of 18,432 spots derived from the same amount of cDNA clones, including 290 spots representing positive and negative control and representing 8606 unigene clusters [79]. These microarrays are the 3rd generation cDNA microarrays designed for *Acropora millepora* [80]. The selection of clones, methodological approach for the cDNA library construction and the fabrication of microarrays are explained in [81].

Hybridization of Arrays

Total RNA was extracted from each sample using Trizol (Invitrogen) following manufacturer's instructions. The integrity and quality of total RNA was assessed using a Bioanalyzer (Agilent Technology). Only samples showing intact RNA (RNA Integrity number >8), were used for probe construction. cDNA probe synthesis was performed from 1000 ng total RNA using Superscript Reverse Transcriptase (Invitrogen) and a 2 pmol Genisphere 900 3DNA Dendrimer from a Genisphere 3DNA-900 microarray kit according to the manufacturers' instructions. We used a reference two-colour microarray design, where, for each array, the sample was labeled with Cy5 and the reference, consisting of pooled RNA from control treatments and time zero, was labeled with Cy3. In total, 27 arrays were hybridized, as each array represented a sample from a treatment and a time point (n = 3), only 3 out of the 4 colonies were used for microarray hybridization. Microarrays were pre-hybridized and hybridized with the labeled samples using the Genisphere 3DNA-900 microarray kit following the manufacturer's instructions and using a dynamic hybridization system (MAUI, BioMicro Systems). Prior to and post hybridization, the microarray slides were washed three times (wash 1: 2×SSC 0.2% SDS at 65°C for 15 min, wash 2: 2×SSC at room temperature for 10 min, wash 3: 0.2×SSC at room temperature for 10 min). Slides were scanned using a GenePix[®] 4200 scanner (Axon Instruments) and image acquisition was performed using the software GenePix[®] Pro 5 (Molecular Devices, CA, USA).

Microarray Analysis

Normalization and data analysis of acquired array slides was performed using R (R Development Core Team, 2008) and the limma package [82]. The details for the methodology of analyzing differential gene expression using empirical Bayes shrinkage of variance and linear regression models can be found in [83]. Normexp (75) corrected signal intensities were used, as it has been

shown to be a well performing background correction method, which best stabilizes variance as a function of intensity, compared to more standard and common methods [84]. Print-tip loess normalization was applied within slides [85] while scale normalization was applied between slides, in order to ensure that distributions were similar between arrays. Both normalization procedures equalize for differing amounts of host RNA input [36]. Effectiveness of normalization procedures was verified through M (the log ratio of the spot fluorescence intensity) vs A (the log of the average spot fluorescence intensity) plots. Minimal or no fluorescence was observed for probes which contained salmon sperm DNA and primers, and should not hybridize, while controls which were expected to hybridize showed a range of fluorescence intensities. Differentially expressed genes were identified based on an assumed false discovery rate of 5% and sequence-wise p-values were adjusted through the Benjamini and Hochberg method [86]. Sets of contrast lists of differentially expressed genes between control, medium and high CO₂ treatments at day 1 and day 28 were created (643 transcripts) (Table S1, Additional file 1), in addition contrast lists were created between groups of samples at t0 so that any potential differences due to "tank effects" could be subtracted from subsequent analysis; in total 3 genes were subtracted from subsequent contrast lists. Differentially expressed genes at day 1 and 28 were then assembled into 6 different clusters based on their temporal gene expression patterns, using K-means clustering analysis in the TIGR TMEV software [87], assuming that genes with similar cellular pathways share common temporal expression patterns. In addition Principal component analysis was also carried out in the TIGR TMEV software [87]. Differentially expressed genes which had homology to known genes (352 transcripts, Blastx, E-score cutoff 10⁻⁶), were assigned to GO categories and subjected to classification analysis using the hypogeometric test and a false discovery rate of 5% in GOEAST [88] to identify enriched GO groups. Microarray data has been deposited in the Gene Expression Omnibus Database (GSE28697).

Validation by Quantitative PCR

Expression patterns of candidate genes from each functional group of coral genes differentially expressed in response to increased CO₂ treatment (sodium and chloride transporter, V type ATPase, vitellogenin, catalase, caspase 3, calmodulin, cytoskeletal actin, pyruvate dehydrogenase, G protein and rab protein) were validated through quantitative Polymerase Chain Reaction (qPCR). Total RNA (1000 ng) was reverse transcribed with a Superscript Vilo cDNA synthesis kit (Invitrogen) following manufacturer's instructions. Specific primers amplifying approximately 100–200 bp PCR products were designed for the genes (Table S4) chosen to be validated from the microarray data. Transcript levels were determined by qPCR using the Corbett Rotor Gene 6000 thermal cycling system (Qiagen), following the manufacturer's instructions (Qiagen, CA, USA) and PCR conditions (95°C for 10 min, followed by 40 cycles of 95°C for 15 sec and 60°C for 1 min). Triplicate first strand diluted 1:10 cDNA aliquots (1 µL) from each sample were used in 20 µL PCR reactions with 2 µM primers and a SYBR Green PCR master mix (Warrington, Cheshire, UK). For each candidate gene control versus high CO₂ samples (4 replicates) at day 28 were tested, as this was the conditions under which major physiological changes occurred, and the greatest differential gene expression was present. A no template control as well as a no reverse transcription control was performed for each gene and treatment to ensure that the cDNA samples did not have DNA contamination. In addition to ensure that gene expression data was representing coral host genes, primer specificity of all primers was tested through PCR

using the qPCR primers and cDNA and genomic DNA from *Symbiodinium* sp. as a template to ensure no amplification. The comparative delta CT method was used to determine relative quantities of mRNA transcripts from each sample. Each value was normalized to two reference genes adenosyl-homocysteinase (AdoHcyase) and ribosomal protein L7 (Rpl7). The selection of reference genes for this experiment was done by using a pool of reference genes (Table S4) and analyzing the expression stability using the GeNorm software [89]. For this study the most stable expression was found for adenosyl-homocysteinase (AdoHcyase) and ribosomal protein L7 (Rpl7) (M value = 0.253) and a minimum of two reference genes was recommended ($V2/3 = 0.126$). Relative expression values were for each gene were calculated by showing a ratio of treatment relative expression over control relative expression on a \log_2 scale, which provides a similar appearance of up and down regulation [41].

Supporting Information

Figure S1 Principal component analysis of gene expression for 3 acidification treatments; control (c), medium (m) and high (h) and 3 time points: T0 (t), day 1 (d) and day 28 (m).
(EPS)

Table S1 Annotated list of differentially expressed transcripts for *Acropora millepora* between CO₂ at day 1 and day 28 (from Additional file 1), as determined by empirical Bayes moderated statistics. Transcripts are assembled into 6 different clusters according to K-means clustering

References

- Lough JM (2008) 10th Anniversary review: a changing climate for coral reefs. *Journal of Environmental Monitoring* 10: 21–61.
- Moberg F, Folke C (1999) Ecological goods and services of coral reef ecosystems. *Ecological Economics* 29: 215–233.
- Hughes TP, Baird AH, Bellwood DR, Card M, Connolly SR, et al. (2003) Climate change, human impacts and the resilience of coral reefs. *Science* 301: 929–933.
- Doney SC, Fabry VJ, Feely RA, Kleypas JA (2009) Ocean acidification: the other CO₂ problem. *Annual Review of Marine Science* 1: 169–192.
- Veron JEN (2008) Mass extinctions and ocean acidification: biological constraints on geological dilemmas. *Coral Reefs* 27: 459–472.
- Kleypas JA, Buddemeier RW, Archer D, Gattuso JP, Langdon C, et al. (1999) Geochemical consequences of increased atmospheric carbon dioxide on coral reefs. *Science* 284: 118–120.
- Hoegh-Guldberg O, Mumby P, Hooten AJ, Steneck RS, Greenfield P, et al. (2007) Coral reefs under rapid climate change and ocean acidification. *Science* 318: 1737–1742.
- Cohen AL, McCorkle DC, de Putron S, Glenn GA, Rose KA (2009) Morphological and compositional changes in the skeletons of new coral recruits reared in acidified seawater: insights into the biomineralization response to ocean acidification. *Geochemistry Geophysics Geosystems* 10: Q07005.
- Pandolfi JM, Connolly SR, Marshall DJ, Cohen AL (2011) Projecting coral reef futures under global warming and ocean acidification. *Science* 333: 418–422.
- Rodolfo-Metalpa R, Houlbrèque F, Tambutte E, Boisson F, Baggini C, et al. (2011) Coral and mollusc resistance to ocean acidification adversely affected by warming. *Nature Climate Change* 1: 308–312.
- Anthony KRN, Kline DI, Diaz-Pulido G, Dove S, Hoegh-Guldberg O (2008) Ocean acidification causes bleaching and productivity loss in coral reef builders. *Proceedings of the National Academy of Sciences of the United States of America* 105: 17442–17446.
- Munday P, Dixon D, Donelson J, Jones G, Pratchett M, et al. (2009) Ocean acidification impairs olfactory discrimination and homing ability of a marine fish. *Proceeding of the National Academy of Science USA* 106: 1848.
- Pörtner HO (2008) Ecosystem effects of ocean acidification in times of ocean warming: a physiologist's view. *Marine Ecology Progress Series* 373: 203–217.
- Weis VM (2008) Cellular mechanisms of Cnidarian bleaching: stress causes the collapse of symbiosis. *Journal of Experimental Biology* 211: 3059–3066.
- Crawley A, Kline DI, Dunn S, Anthony KRN, Dove S (2010) The effect of ocean acidification on symbiont photorespiration and productivity in *Acropora formosa*. *Global Change Biology* 15: 851–197.
- Muscatine L, McCloskey LR, Marian RE (1981) Estimating the daily contribution of carbon from zooxanthellae to coral animal respiration. *Limnology and Oceanography* 26: 601–611.
- Guppy M, Withers P (1999) Metabolic depression in animals: physiological perspectives and biochemical generalizations. *Biological Reviews* 74.
- Grosser J, Schrecker O, Greten H (1981) Function of hepatic triglyceride lipase in lipoprotein metabolism. *Journal of Lipid Research* 22: 437–442.
- Thorpe C, Kim JJP (1995) Structure and mechanism of action of the Acyl-CoA dehydrogenases. *The FASEB Journal* 9: 718–725.
- Matsuyama S, Reed JC (2000) Mitochondria-dependent apoptosis and cellular pH regulation. *Cell Death and Differentiation* 7: 1155–1165.
- Todgham AE, Hofmann GE (2009) Transcriptomic response of sea urchin larvae *Strongylocentrotus purpuratus* to CO₂ driven seawater acidification. *Journal of Experimental Biology* 212: 2579–2594.
- Muscatine L (1990) The role of symbiotic algae in carbon and energy flux in reef corals. In: Dubinsky Z, ed. *Coral Reefs* Amsterdam: Elsevier. pp 75–87.
- Grottoli AG, Rodrigues LJ, Palardy JE (2006) Heterotrophic plasticity and resilience in bleached corals. *Nature* 440: 1186–1189.
- Obara M, Szeliga M, Albrecht J (2008) Regulation of pH in the mammalian central nervous system under normal and pathological conditions: Facts and hypotheses. *Neurochemistry International* 52: 905–919.
- Heisler N (1989) Interactions between gas exchange, metabolism and ion transport in animals: an overview. *Canadian Journal of Zoology* 67: 2923–2934.
- Huertas IE, Colman B, Espie GS (2002) Mitochondrial-driven bicarbonate transport supports photosynthesis in marine microalgae. *Plant Physiology* 130: 284–291.
- von Heijne G (2007) The membrane protein universe: what's out there and why bother? *Journal of Internal Medicine* 261: 543–557.
- Jones PM, George AM (2004) The ABC transporter structure and mechanism: perspectives on recent research. *Cellular and Molecular Life Sciences* 61: 682–699.
- Hinton A, Sennoune SR, Bond S, Fang M, Reuveni M, et al. (2009) Function of a subunit of the V-ATPase in pH homeostasis and in vitro invasion of MDA-MB231 human breast cancer cells. *Journal of Biological Chemistry* 284: 16400–16408.
- Furla P, Allemann D, Orsenigo M (2000) Involvement of H⁺-ATPase and carbonic anhydrase in inorganic carbon uptake for endosymbiont photosynthesis. *American Journal of Physiology: Regulatory Integrative Comparative Physiology* 278: R870–R881.
- Pörtner HO, Book C, Reipschläger A (2000) Modulation of the cost of pH regulation during metabolic depression: a ³¹P-NMR study in invertebrate (*Sipunculus nudus*) isolated muscle. *Journal of Experimental Biology* 203: 2417–2428.
- Petrackova D, Vecer J, Svoboda J, Herman P (2010) Long-term adaptation of *Bacillus subtilis* 168 to extreme pH affects chemical and physical properties of the cellular membrane. *Journal of Membrane Biology* 233: 73–83.

33. Kültz D (2005) Molecular and evolutionary basis of the cellular stress response. *Annual Review of Physiology* 67: 225–257.
34. DeSalvo MK, Voolstra CR, Sunagawa S, Schwarz JA, Stillman JH, et al. (2008) Differential gene expression during thermal stress and bleaching in the Caribbean coral *Montastraea faveolata*. *Mol Ecol* 17: 3952–3971.
35. Lesser MP, Farrell JH (2004) Exposure to solar radiation increases damage to both host tissues and algal symbionts of corals during thermal stress. *Coral Reefs* 23: 367–377.
36. DeSalvo MK, Sunagawa S, Voolstra CR, Medina M (2010) Transcriptomic responses to heat stress and bleaching in the elkhorn coral *Acropora palmata*. *Marine Ecology Progress Series* 402: 97–113.
37. Dunn SR, Phillips WS, Spatafora JW, Green DR, Weis VM (2006) Highly conserved Caspase and Bcl-2 homologues from the sea anemone *Aiptasia pallida*: lower metazoans as models for the study of apoptosis evolution. *Journal of Molecular Evolution* 63: 95–107.
38. Hauer J, Püschner S, Ramakrishnan P, Simon U, Bongers M, et al. (2005) TNF receptor (TNFR)-associated factor (TRAF) 3 serves as an inhibitor of TRAF2/5 mediated activation of the noncanonical NF- κ B pathway by TRAF-binding TNFRs. *Proceeding of the National Academy of Science USA* 22: 2874–2879.
39. Lankat-Buttgereit B, Goke R (2009) The tumour suppressor Pcdcd4: recent advances in the elucidation of function and regulation. *Biology of the Cell* 101: 309–317.
40. Kraus ZJ, Haring JS, Bishop GA (2008) TNF receptor-associated factor 5 is required for optimal T cell expansion and survival in response to infection. *Journal of Immunology* 181: 7800–7809.
41. Pernice M, Dunn SR, Miard T, Dufour S, Dove S, et al. (2011) Regulation of apoptotic mediators reveals dynamic responses to thermal stress in the reef building coral *Acropora millepora*. *PLoS One* 6: e16095.
42. Uren AG, O'Rourke K, Aravind L, Pisabarro MT, Seshagiri S, et al. (2000) Identification of paracaspases and metacaspases: two ancient families of caspase-like proteins, one of which plays a key role in MALT lymphoma. *Molecular Cell* 6: 961–967.
43. Hirayama H, Seino J, Kitajima Y, Jigami Y, Suzuki T (2010) Free oligosaccharides to monitor glycoprotein endoplasmic reticulum-associated degradation in *Saccharomyces cerevisiae*. *Journal of Biological Chemistry* 285: 12390–12404.
44. Li Y, Bergeron JJM, Luo L, Ou WJ, Thomas DY, et al. (1996) Effects of inefficient cleavage of the signal sequence of HIV-1 gp120 on its association with calnexin, folding, and intracellular transport. *Proceeding of the National Academy of Science USA* 93: 9606–9611.
45. Kvennefors ECE, Leggat W, Hoegh-Guldberg O, Degnan BM, Barnes AC (2008) An ancient and variable mannose-binding lectin from the coral *Acropora millepora* binds both pathogens and symbionts. *Developmental and Comparative Immunology* 32: 1582–1592.
46. Rosenberg E, Koren O, Reshef L, Efrony R, Zilber-Rosenberg I (2007) The role of microorganisms in coral health, disease and evolution. *Nature Reviews Microbiology* 5: 355–362.
47. Miller DJ, Hemmrich G, Ball EE, Hayward DC, Khalturin K, et al. (2007) The innate immune repertoire in Cnidaria - ancestral complexity and stochastic gene loss. *Genome Biology* 8: R59.
48. Schwarz JA, Brokstein PB, Voolstra CR (2008) Coral life history and symbiosis: functional genomic resources for two reef building Caribbean corals, *Acropora palmata* and *Montastraea faveolata*. *BMC Genomics* 9: 97.
49. Hidalgo C (2005) Cross talk between Ca²⁺ and redox signaling cascades in muscle and neurons through the combined activation of ryanodine receptors/ Ca²⁺ release channels. *Philosophical Transactions of the Royal Society of London Series B: Biological Sciences* 360: 2237–2246.
50. Kasri NN, Parys JB, Callewaert G, Missiaen L, De Smedt H (2004) Calmodulin and calcium-release channels. *Biological Research* 37: 577–582.
51. Schallreuter KU, Gibbons NC, Zothner C, Abou Elloof MM, Wood JM (2007) Hydrogen peroxide mediated oxidative stress disrupts calcium binding on calmodulin: more evidence for oxidative stress in vitiligo. *Biochemical and Biophysical Research Communications* 360: 70–75.
52. Fill M, Capello JA (2002) Ryanodine receptor calcium release channels. *Physiological Reviews* 82: 893–922.
53. Croall D, Ersfeld K (2007) The calpains: modular designs and functional diversity. *Genome Biology* 8: 218.
54. Doherty GJ, McMahon HT (2008) Mediation, modulation and consequences of membrane-cytoskeleton interactions. *Annual Review of Biophysics* 37: 65–95.
55. Zheng B, Han M, Bernier M, Wen JK (2009) Nuclear actin and actin-binding proteins in the regulation of transcription and gene expression. *The FEBS journal* 276: 2669–2685.
56. Dollar GL, Weber U, Mlodzik M, Sokol SY (2005) Regulation of Lethal giant larvae by Dishevelled. *Nature* 437: 1376–1380.
57. Shima DT, Scales SJ, Kreis TE, Pepperkok R (1999) Segregation of COPI rich and anterograde cargo rich domains in endoplasmic reticulum to Golgi transport complexes. *Current Biology* 9: 821–824.
58. Whitley NM, Scott JL, Breeze SJ, McCann L (2001) Effects of water salinity on acid-base balance in decapod crustaceans. *Journal of Experimental Biology* 204: 1003–1011.
59. Hoeflich KP, Ikura M (2004) Radixin: cytoskeletal adaptor and signaling protein. *International Journal of Biochemistry & Cell Biology* 36: 2131–2136.
60. Lees-Miller JP, Helfman DM, Schroer TA (1992) A vertebrate actin-related protein is a component of a multisubunit complex involved in microtubule-based vesicle motility. *Nature* 359: 244–246.
61. Cully M, Downward J (2008) SnapShot: Ras Signaling. *Cell* 133: 1292.
62. Pfeiffer S, Aivazian D (2004) Targeting Rab GTPases to distinct membrane compartments. *Nature Reviews Molecular Cell Biology* 5: 886–896.
63. Stenmark H, Olkkonen VM (2001) The Rab GTPase family. *Genome Biology* 2: 3007.3001–3007.3007.
64. Cadenas E, Davies KJ (2000) Mitochondrial free radical generation, oxidative stress, and aging. *Free Radical Biology and Medicine* 29: 222–230.
65. Davidson JF, Schiestl RH (2001) Mitochondrial respiratory electron carriers are involved in oxidative stress during heat stress in *Saccharomyces cerevisiae*. *Molecular and Cellular Biology* 21: 8483–8489.
66. Muller J, Menzel D, Samaj J (2007) Cell-type specific disruption and recovery of the cytoskeleton in *Arabidopsis thaliana* epidermal root cells upon heat shock stress. *Protoplasma* 230: 231–242.
67. Dunn SR (2009) Immunorecognition and immunoreceptors in the Cnidaria. *Invertebrate Survival Journal* 6: 7–14.
68. Orrenius S, Zhivotovskiy B, Nicotera P (2003) Regulation of cell death: the calcium-apoptosis link. *Nature Reviews Molecular Cell Biology* 4: 552–565.
69. Caldeira K, Wickett ME (2003) Anthropogenic carbon and ocean pH. *Nature* 425: 365.
70. Pelejero C, Calvo E, Hoegh-Guldberg O (2010) Paleo-perspective on ocean acidification. *Trends in Ecology & Evolution* 25: 332–345.
71. Dickson AG, Afghan JD, Andersen GC (2003) Reference materials for oceanic CO₂ analysis: a method for the certification of total alkalinity. *Marine Chemistry* 80: 185–197.
72. Mehrbach C, Culbertson CH, Hawley JE, Pytkowicz RM (1973) Measurement of the apparent dissociation constants of carbonic acid in seawater at atmospheric pressure. *Limnology and Oceanography* 18: 897–907.
73. Dickson AG, Millero FJ (1987) A comparison of the equilibrium constants for the dissociation of carbonic acid in seawater media. *Deep Sea Research* 34: 1733–1743.
74. Lewis E, Wallace DWR (1998) Program developed for CO₂ system calculations. In: Carbon Dioxide Information Analysis Center ORNL, US., editor. Oak Ridge, TN: Department of Energy.
75. Barnes D, Chalker B (1990) Calcification and photosynthesis in reef-building corals and algae. In: Z. D, ed. *Ecosystems of the World: Vol 25, Coral Reefs*. Amsterdam: Elsevier Science. pp 109–131.
76. Zapata M, Rodriguez F, Garrido JL (2000) Separation of chlorophylls and carotenoids from marine phytoplankton: a new HPLC method using a reversed-phase C8 column and pyridine-containing mobile phases. *Marine Ecology Progress Series* 195: 29–45.
77. Stimson J, Kinzie RA (1991) The temporal pattern and rate of release of zooxanthellae from the reef coral *Pocillopora damicornis* (Linnaeus) under nitrogen-enrichment and control conditions. *Journal of Experimental Marine Biology and Ecology* 153: 63–74.
78. Spencer-Davies P (1989) Short-term growth measurements of coral growth using an accurate buoyant weighing technique. *Marine Biology* 101: 389–395.
79. Bay LK, Ulstrup KE, Nielsen HB, Jarmer H, Goffard N, et al. (2009) Microarray analysis reveals transcriptional plasticity in the reef building coral *Acropora millepora*. *Mol Ecol* 18: 3062–3075.
80. Foret S, Kassahn KS, Grasso LC, Hayward DC, Iguchi A, et al. (2007) Genomic and microarray approaches to coral reef conservation biology. *Coral Reefs* 26: 475–486.
81. Grasso LC, Maimondal J, Rudd S, Hayward DC, Saint R, et al. (2008) Microarray analysis identifies candidate genes for key roles in coral development. *BMC Genomics* 9: 540.
82. Smyth GK (2005) Limma: Linear models for microarray data. In: W H, ed. *In: Bioinformatics and Computational Biology Solutions using R and Bioconductor*. New York: Springer. pp 397–420.
83. Smyth GK (2004) Linear models and empirical Bayes methods for assessing differential expression in microarray experiments. *Statistical Applications in Genetics and Molecular Biology* 3: Article 3.
84. Ritchie ME, Silver J, Oshlack A, Holmes M, Diyagama D, et al. (2007) A comparison of background correction methods for two-colour microarrays. *Bioinformatics* 23: 2700–2710.
85. Smyth GK, Speed T (2003) Normalization of cDNA microarray data. *Methods* 31: 265–273.
86. Benjamini Y, Hochberg Y (1995) Controlling the false discovery rate: a practical and powerful approach to multiple testing. *Journal of the Royal Statistical Society Series B* 57: 289–300.
87. Saeed AI, Sharov V, White J, Li J, Liang W, et al. (2003) TM4: a free, open-source system for microarray data management and analysis. *BioTechniques* 34: 374–378.
88. Zheng Q, Wang XJ (2008) GOEAST: a web-based software toolkit for gene ontology enrichment analysis. *Nucleic Acids Research* 36: W358–363.
89. Vandesompele J, De Preter K, Pattyn F, Poppe B, Van Roy N, et al. (2002) Accurate normalization of real-time quantitative RT-PCR data by geometric averaging of multiple control genes. *Genome Biology* 3: 6906–6914.